



Article

Integrated Design of Structure and Material of Epoxy Asphalt Mixture Used in Steel Bridge Deck Pavement

Wen Nie ^{1,2,*} , Duanyi Wang ¹, Yangguang Sun ³, Wei Xu ¹  and Xiaoquan Xiao ²

¹ School of Civil Engineering and Transportation, South China University of Technology, 381 Wushan Road, Tianhe District, Guangzhou 510641, China; tcdywang@scut.edu.cn (D.W.); xuweib@scut.edu.cn (W.X.)

² Xiaoning Institute of Roadway Engineering, Wushan Road, Tianhe District, Guangzhou 510641, China; oyeoye@21cn.com

³ Guangdong Communication Planning & Design Institute Group Co., Ltd., 22 Xinghua Road, Tianhe District, Guangzhou 510507, China; syga1200@163.com

* Correspondence: 202010101505@mail.scut.edu.cn; Tel.: +86-134-2757-0198

Abstract: To comprehensively investigate the integrated structural and material design of the epoxy asphalt mixture used in steel bridge deck pavement, the following works have been conducted: 1. The strain level of steel bridge deck pavement was calculated; 2. The ultimate strain level of fatigue endurance for epoxy asphalt concrete was measured; 3. The effect of water tightness of epoxy asphalt mixture on the bonding performance of steel plate interface was tested. 4. For better performance evaluation, quantitative analysis of the anti-skid performance of epoxy asphalt mixture was carried out by testing the structure depth using a laser texture tester. Results show the following findings: 1. The fatigue endurance limit strain level of epoxy asphalt mixture ($600 \mu\epsilon$) was higher than that of the steel bridge deck pavement ($<300 \mu\epsilon$), indicating that the use of epoxy asphalt concrete has better flexibility and can achieve a longer service life in theory; 2. The epoxy asphalt concrete has significant water tightness to protect the steel plate interface from corrosion and ensure good bonding performance; 3. The porosity of epoxy asphalt mixture used in steel bridge deck paving should be controlled within 3%; 4. In terms of anti-skid performance of bridge deck pavement, the FAC-10 graded epoxy asphalt mixture is recommended when compared with EA-10C.

Keywords: epoxy asphalt mixture; steel bridge deck; structure and material; fatigue durability performance; bonding performance; anti-skid performance



Citation: Nie, W.; Wang, D.; Sun, Y.; Xu, W.; Xiao, X. Integrated Design of Structure and Material of Epoxy Asphalt Mixture Used in Steel Bridge Deck Pavement. *Buildings* **2022**, *12*, 9. <https://doi.org/10.3390/buildings12010009>

Academic Editors: Xiaopei Cai, Huayang Yu and Tao Wang

Received: 23 November 2021

Accepted: 21 December 2021

Published: 23 December 2021

Publisher's Note: MDPI stays neutral with regard to jurisdictional claims in published maps and institutional affiliations.



Copyright: © 2021 by the authors. Licensee MDPI, Basel, Switzerland. This article is an open access article distributed under the terms and conditions of the Creative Commons Attribution (CC BY) license (<https://creativecommons.org/licenses/by/4.0/>).

1. Introduction

The pavement of long-span steel bridge decks is a worldwide engineering and technical difficulty. The pavement structure must have a certain degree of following deformation with the steel plate, water tightness, and anti-skid performance to ensure its requirements on durability and function [1,2].

Guangdong Province is located in tropical and subtropical regions with year-round high temperatures and rainfall, especially near the Pearl River Estuary, where it is quite hot, rainy, humid, and highly salty all year round. Therefore, strict requirements are imposed on how to protect the steel plate of the steel bridge deck from corrosion, as well as the anti-skid performance to ensure safe driving in rainy weather [3,4].

Epoxy asphalt is a mixture of epoxy resin, curing agent, and base asphalt through chemical reactions [5–7]. The epoxy asphalt mixture is a kind of thermosetting concrete material made from epoxy asphalt as a binder and mineral materials that meet the grading requirements according to a specific process [8,9]. It is proved from practice that traditional epoxy asphalt concrete has a higher modulus than other asphalt concretes [10–12], but it has a relatively low toughness [13–15], that is, the following deformation of traditional epoxy asphalt mixture and steel plate is relatively low.

Asphalt concrete for the pavement layer needs to ensure excellent fatigue resistance and anti-skid performance [16–20]. As a composite structural system, it is necessary

to ensure the integrity of the pavement layer and the orthotropic steel plate, the water tightness and waterproofness [21,22], the anti-corrosion performance [23,24], and the adhesion performance [10], which are the key links to ensuring the integrity of the steel bridge deck pavement [15,25].

In 1973, the American AASHTO Bridge Design Code was included for the first time in terms of design for orthotropic steel bridge decks [26]. However, in this code, as well as subsequent versions and technical documents, there is almost no information on bridge deck paving requirements and design guidance. There is a disconnect between the structural design of the steel deck pavement and the material design, and there are concerns about the performance of the pavement materials, leading to frequent problems such as lack of fatigue durability of the steel deck pavement, frequent early diseases and lack of anti-skid performance [1,27–30].

Based on the steel deck paving project of Nansha Bridge in Guangdong Province, the author analyzes the maximum strain level of the steel deck of the Dasha Waterway Bridge (1200 m) of the Nansha Bridge by establishing a finite element computing model, and then the four-point bending fatigue test is used to determine the ultimate strain level of fatigue endurance for the epoxy asphalt mixture. The two values are compared to verify whether the following deformation of the epoxy asphalt mixture meets the requirements; the interface fracture ratio of epoxy asphalt mixture with different porosity and the bonding layer is collected through pull test, so as to analyze the water tightness effect of epoxy asphalt mixture of steel bridge deck pavement; the anti-skid performance is optimized through the grade study of epoxy asphalt mixture, so as to carry out the integrated design of structure and materials for epoxy asphalt mixture in steel bridge deck pavement.

2. Research on Deformation Performance of Mixture following Steel Plate

To determine the stress and deformation characteristics of the steel bridge deck pavement, the numerical simulation and computing analysis should be firstly carried out on the bridge deck. The analysis of local deformation of the bridge deck from the entire bridge model requires high computer requirements and low calculation efficiency; if the independent beam section is analyzed, there is a lack of effective simulation of the role of the entire bridge; the application of the submodel method can effectively solve this contradiction. When analyzing the local response of the bridge deck under wheel load, the coarser element mesh generation is first used to analyze the overall force state of the structure, and then the local structure to be analyzed is selected to subdivide the element mesh according to the force state distribution, and the partial beam segment submodel is established. The boundary conditions of the submodel are determined by the displacement interpolation of the corresponding position nodes in the overall structure.

2.1. Conditions and Content of Mechanical Calculation and Analysis

2.1.1. Load Conditions

The stress of steel bridge deck pavement is mainly manifested in the fatigue damage caused by the repeated action of wheel load [25,26,31,32]. The stress and deformation characteristics of the bridge deck pavement at representative positions under general operating conditions are analyzed to reflect the general force level of the steel deck pavement and provide a reference for paving design [33,34]. Considering those pavement materials, as viscoelastic materials, have stress relaxation characteristics, the ultimate deformation of the deck structure of a general bridge is much lower than the strength and fatigue limit of the pavement materials. Besides, the probability and frequency of most unfavorable load conditions of the overall structure of the pavement bridge are quite low. Therefore, the most unfavorable deformation of the overall structure of the bridge is not considered as key analysis content.

Considering that the steel bridge deck pavement is mainly concerned with fatigue damage and destruction, it is necessary to simulate the general operating state of the bridge. In the calculation model, the load condition of four parallel traffic lanes is applied

according to JTGD60-2015 [32]. The load is 10.5 kN/m, the impact coefficient is 0.05, the longitudinal reduction factor is 0.93, and the transverse reduction factor is 0.5. The overall model is used to determine the beam section with a higher transverse strain, which will be a representative position for a detailed analysis of the sub-model pavement force.

In the sub-model, standard vehicles are arranged horizontally in four parallel traffic lanes. As for the vertical direction, the influence of the diaphragm position is considered. Besides, a concentrated load of vehicles is applied in the sub-model, and the surface load is applied according to the four tire contact surfaces of $2 \times 200 \text{ mm} \times 200 \text{ mm} + 2 \times 200 \text{ mm} \times 200 \text{ mm}$. Four standard vehicles are arranged parallel in the horizontal direction. In the longitudinal direction, the load is placed near the unfavorable position of the transverse bulkhead. A local vehicle load is considered as a form of unfavorable working conditions.

2.1.2. Calculation Model and Analysis Method

In this study, the sub-model method is used to analyze the strain distribution law of the steel bridge deck pavement. In this method, a beam section of 18 m long and half the width of the bridge is taken as the sub-model. Furthermore, the sub-model introduces the boundary conditions of the corresponding position of the calculation result of the whole bridge model. In addition, the shell element is used to simulate the box girder steel plate, and the link element is used to simulate the main cable, stay cable, and sling. It is worth noting that the bridge deck pavement is not covered by the first-stage load deformation.

As the pavement under vehicle load mainly exhibits instantaneous elastic response, the elastic static force should be calculated assuming that the paving material is elastic [33,35]. The pavement layer and the steel bridge deck are completely continuous integrated structures [36]. Meanwhile, the pavement layer bridges account for a small proportion of the overall stiffness. Thus, the pavement layer is not modeled separately in the overall model, and 3D elements are used to simulate the pavement layer in the sub-model.

2.1.3. Calculation and Analysis Content

The investigation shows that the longitudinal fatigue cracking of steel bridge deck pavement caused by transverse strain is generally distributed in the wheel track zone, and the longitudinal position is randomly distributed throughout the bridge [32]. It is necessary to focus on the analysis of the transverse strain of the pavement layer and analyze the fatigue resistance requirements of the pavement layer according to the stress state of the pavement layer [34].

Analyze the influence of axle load and pavement modulus on the stress state of the pavement structure. The axle load is calculated as 100 kN, 140 kN, and 200 kN. The pavement modulus is, respectively, taken as 2000 MPa, 5000 MPa, and 10,000 MPa, considering that the pavement modulus is affected by temperature.

2.2. Finite Element Calculation and Analysis

Taking the main project of the Dasha Waterway Bridge of Nansha Bridge as an example, a two-tower three-span suspension bridge with a main span of 1200 m has a rise-to-span ratio of 1:9.65, a center-to-center spacing of the main cables in the transverse direction of 42.1 m, and a standard spacing of slings along the bridge of 12.8 m, the thickness of the steel plate of 16 mm. The restraint system of the stiffening beam is provided with transverse wind-resistant bearings at the transition piers and pylons; longitudinal limit damping devices are installed at the two pylons; vertical tension and compression bearings are installed at the two transition piers.

2.2.1. Numerical Calculation Model

The ANSYS finite element analysis software is used to calculate the stress state of the bridge deck pavement [37]. The parameters of steel box girder plate size, material modulus, and Poisson's ratio are shown in Table 1. Box girder model roof, U-shaped stiffeners, diaphragms, and other steel plate structures adopt shell elements, pavement

layers adopt solid elements, and cables adopt link elements. The calculation assumes that the pavement layer is a completely continuous Isotropic elastomer, the interlayer contact between the pavement layer and the steel plate is completely continuous. Boundary conditions: constraints shall be set according to the bridge design drawings. In terms of the vehicle-mounted model of the local load on the bridge deck pavement, the double-wheel set with the axle load of 100 kN required in the highway pavement design standard was adopted as the standard load, namely BZZ-100. The double-wheel landing areas are two squares in $200\text{ mm} \times 200\text{ mm}$ with a spacing of 100 mm, and the General Specification for Design of Highway Bridges and Culverts are referred to compare and analyze the axle load 140 kN, and the axle load is 200 kN for overload.

Table 1. Numerical model parameters of bridge deck pavement.

Item	Size Parameter/mm	Elastic Modulus/MPa	Poisson's Ratio
Steel plate	Design thickness	210,000	0.3
Thickness of paving layer	65	2000, 5000, 10,000	0.25

The finite element calculation model of the whole bridge takes half the width in the transverse direction and the calculation amount is reduced by symmetrical structure and symmetric loading; the submodel is a section of 18 m along the longitudinal bridge direction. Through the ANSYS finite element analysis software, the schematic diagrams of finite element calculation model are shown in Figures 1–5 (X refers to the horizontal direction; Z refers to the longitudinal direction; Y refers to the vertical direction, similarly hereinafter).

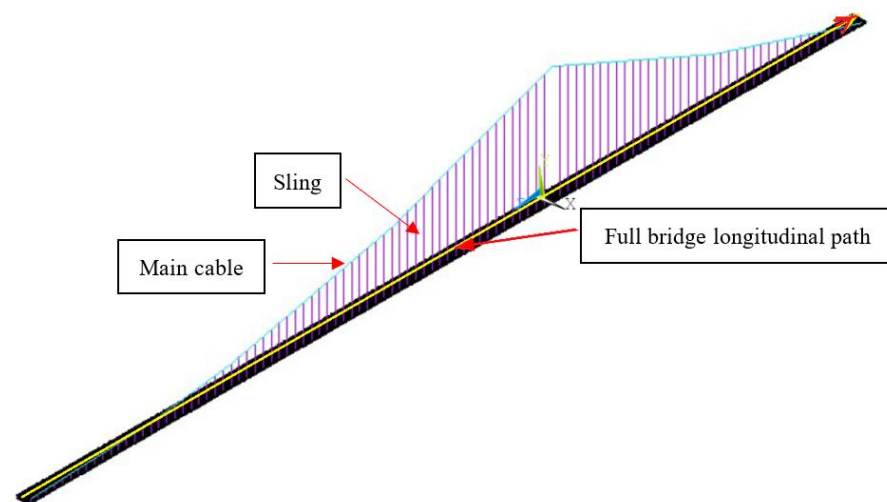


Figure 1. Numerical simulation and calculation model of Dasha Waterway Bridge of Nansha Bridge.

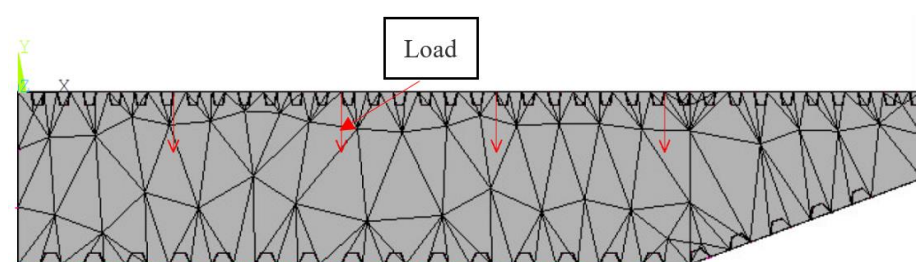


Figure 2. Cross section of box girder of the numerical simulation and calculation model in Nansha Bridge Dasha Waterway Bridge.

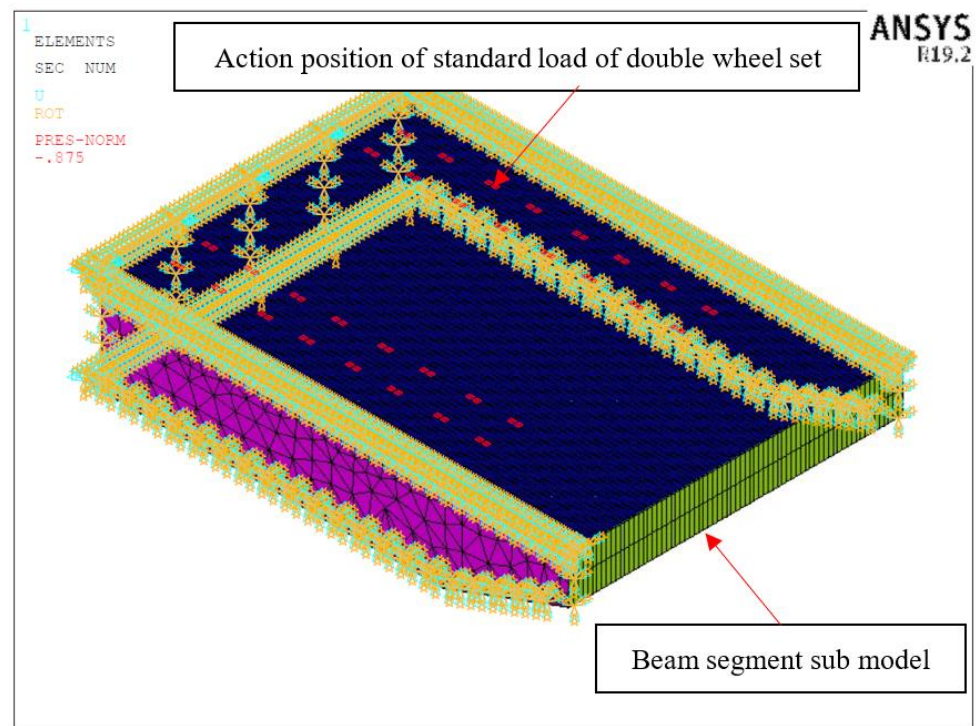


Figure 3. Numerical simulation and calculation model of partial beam segment submodel in Nansha Bridge Dasha Waterway Bridge.

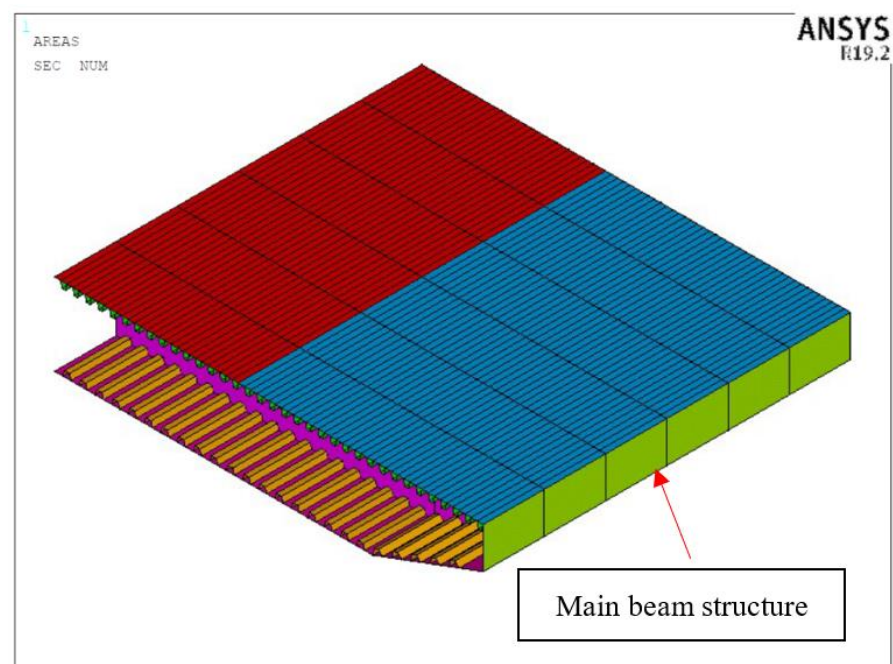


Figure 4. Numerical simulation of steel bridge deck girder structure diagram.

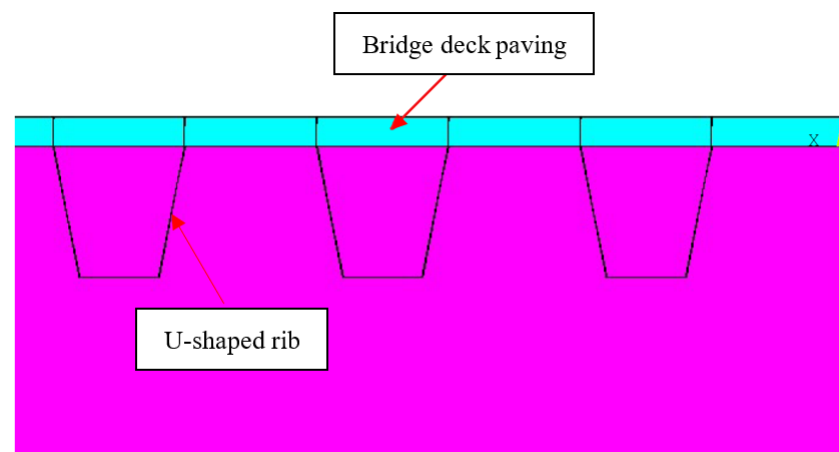


Figure 5. Numerical simulation of composite structure of steel bridge deck pavement.

2.2.2. Analysis of Force Data of Steel Bridge Deck Pavement

The analysis data of the highest tensile strain, compressive strain, and their difference (PP peak amplitude) of the surface strain of the pavement layer are shown in Table 2. The PP peak amplitude is the difference amplitude between the maximum tensile strain and the compressive strain at a distance of 300 mm.

Table 2. Strain analysis data of pavement layer surface.

Model Parameters	Axle Load (kN)	Modulus of Pavement Layer (MPa)	Transverse Strain of Top Surface of Pavement Layer ($\times 10^{-6}$)
Maximum value (tensile strain)	100	2000	146
		5000	100
		1000	75
	140	2000	178
	200	2000	280
Lowest value (compressive strain)	100	2000	−166
		5000	−102
		10,000	−51
	140	2000	−249
PP peak amplitude	100	2000	312
		5000	202
		10,000	126
	140	2000	427

The top surface maximum tensile strain for 100 kN axle load and pavement modulus with 2000 MPa, 5000 MPa, and 10,000 MPa pavement are 146 $\mu\epsilon$, 100 $\mu\epsilon$, and 75 $\mu\epsilon$, the top surface maximum tensile strain for 100 kN, 140 kN, and 200 kN axle load and pavement modulus with 2000 MPa pavement are 146 $\mu\epsilon$, 178 $\mu\epsilon$, and 280 $\mu\epsilon$, respectively. The data show that the tensile strain level decreases as the pavement modulus increases, and the tensile strain level increases as the axle load increases.

The top surface maximum compressive strains for 100 kN axle load and pavement modulus with 2000 MPa, 5000 MPa, 10,000 MPa pavement are 166 $\mu\epsilon$, 102 $\mu\epsilon$, and 51 $\mu\epsilon$, the top surface maximum compressive strains for 100 kN and 140 kN axle load and pavement modulus with 2000 MPa pavement are, respectively, 166 $\mu\epsilon$ and 249 $\mu\epsilon$. The data show

that the compressive strain level decreases as the pavement modulus increases, and the compressive strain level increases as the axle load increases.

The maximum tensile strain of the pavement top surface and the maximum compressive strain difference (PP peak amplitude) of the adjacent area (300 mm) data for 100 kN axle load and pavement modulus with 2000 MPa, 5000 MPa, and 10,000 MPa are 312 $\mu\epsilon$, 202 $\mu\epsilon$, 126 $\mu\epsilon$, the maximum tensile strain difference (PP peak amplitude) of the pavement top surface and the maximum compressive strain of the adjacent area (300 mm) for 100 kN and 140 kN axle load and 2000 MPa pavement modulus are 312 $\mu\epsilon$ and 427 $\mu\epsilon$.

2.3. Fatigue Durability of Epoxy Asphalt Mixture

The fatigue test evaluation of the hot-mix epoxy asphalt mixture is carried out, and the fatigue performance of the epoxy asphalt mixture is studied on the Cooper four-point bending fatigue testing machine. The diabase gravel and the mineral powder were used in this test, which was supplied by Furong Quarry, Heyuan, Guangdong, China. The EC-10C gradation was used and the best oil-stone ratio of EA-10C (6.5%) was determined through the design of the mix ratio. According to JTG E20 T0739-2011, standard size 380 mm \times 63.5 mm \times 50 mm small beam specimens were prepared for the four-point bending fatigue test. In this test, the test temperature was 15 $^{\circ}\text{C}$, the loading frequency was 10 Hz, and the loading strain level was 600 $\mu\epsilon$.

The material stiffness modulus dropped to 50% of the initial stiffness modulus was taken as the fatigue failure criterion. The curve of the flexural stiffness modulus ratio of epoxy asphalt mixture with the number of loading actions is shown in Figure 6, which shows that when the strain level is 600 $\mu\epsilon$, the fatigue life is more than 10 million times. Under this strain level test condition, the hot-mixed epoxy asphalt mixture exhibits a fatigue endurance limit.

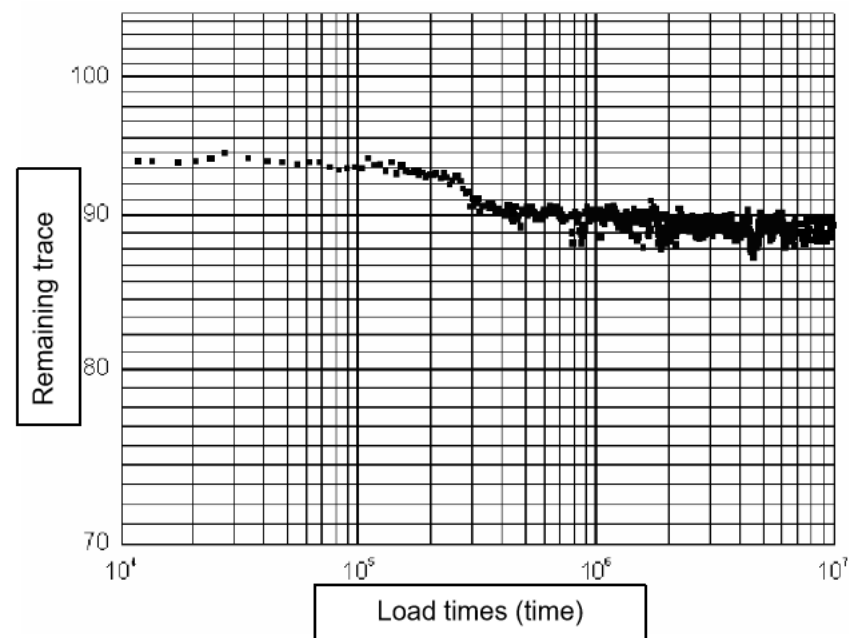


Figure 6. Fatigue endurance test curve of epoxy asphalt mixture.

Hot-mix epoxy asphalt mixture is a viscoelastic material [38]. As the fatigue test temperature increases, its fatigue resistance also increased significantly [39]. The endurance limit strain level of hot-mix epoxy asphalt at 15 $^{\circ}\text{C}$, 30 $^{\circ}\text{C}$, and 60 $^{\circ}\text{C}$ are shown in Figure 7.

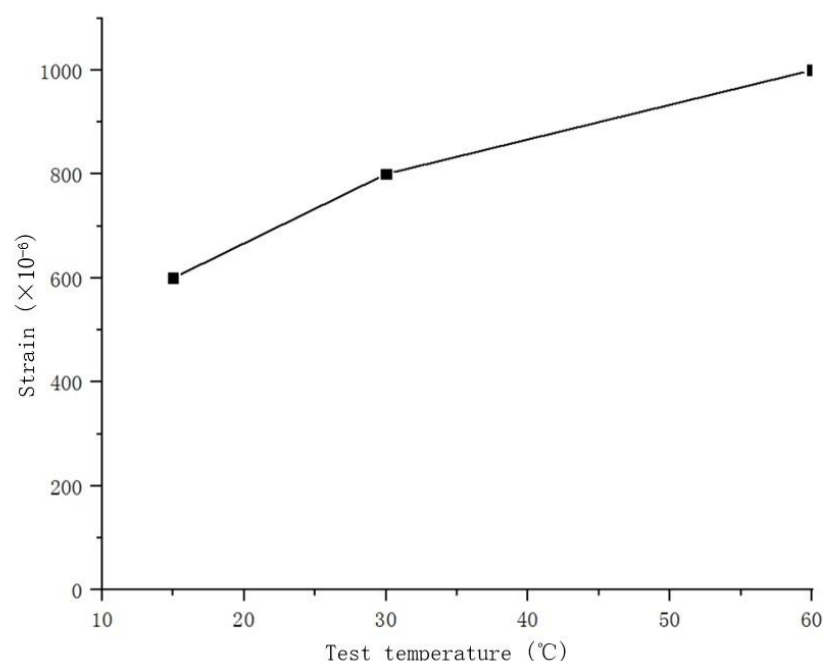


Figure 7. Fatigue endurance ultimate strain level of epoxy asphalt mixture at different test temperatures.

See Table 2 for the maximum tensile strain data of the top surface of the pavement layer under the conditions of axle load 100 kN and 200 kN (overload) and 2000 MPa modulus of the pavement layer. Under relatively unfavorable conditions, the tensile strain on the top surface of the pavement layer is lower than 300 $\mu\epsilon$, and the maximum PP peak amplitude is 427 $\mu\epsilon$, which is significantly lower than the 600 $\mu\epsilon$ fatigue endurance limit of hot-mix epoxy asphalt concrete.

Therefore, in terms of flexural and tensile fatigue performance, the use of hot-mix epoxy asphalt concrete for steel bridge deck pavement can achieve a longer life in theory.

3. Research on the Effect of Water Tightness on Interfacial Bonding Performance

To study the effect of the water tightness of the epoxy asphalt mixture on the bonding performance of the steel plate interface, the composite structure of “steel plate + epoxy resin bonding layer + hot-mix epoxy asphalt mixture” is adopted, and the porosity for epoxy asphalt mixture adopts 1.5%, 3.0%, 4.5%, and 6.0%. By setting four kinds of composite structures with different porosity, the influence of different water tightness of epoxy asphalt mixture on the bonding performance of steel plate interface was studied. There are eight rutting test pieces of each composite structure with a total of 32 rutting test pieces. The epoxy asphalt mixture adopts EA-10 (F) with single-layer paving, the total thickness of the steel plate is 50 mm, and the epoxy resin bonding layer is 0.4 kg/m².

Whether high temperature loading and salt spray erosion are set up for comparison tests is according to different test temperatures. The interface fracture ratio of epoxy asphalt mixture with different porosity and the bonding layer is collected through the pull test, to analyze the water tightness effect of the epoxy asphalt mixture of the steel bridge deck pavement and observe the corrosion of the steel plate under different conditions.

3.1. Pull Test

In this research, two groups, including the comparison group and the high temperature loading and salt spray erosion group, were set. Before the pull test, following JTG E20 T0719-2011 and GB/T 10125-2012, the composite structure specimens with different porosity of the high temperature loading and salt spray erosion group were subjected to a continuous 10 h rutting test at 60 °C (simulating the repeated action of a vehicle on the paving layer under high temperature conditions) and a 15 d salt spray test (simulating the long-term

erosion of the paving layer by salt spray). Then the composite structure specimens of the comparison group and the high temperature loading and salt spray erosion group were drilled and subjected to a pull test, respectively. In the pull test, a fully automatic digital display pull-out adhesion tester was used, and the test temperatures were set at 25 °C and 60 °C, respectively.

Each group is subjected to eight pull tests. The results of the pull test are divided into two types according to the different fracture surfaces. The first type of fracture surface is the interface between the bonding layer and the mixture, and the other type is the interior of the mixture as shown in Figure 8. See Table 3 for the number of interface disconnections between the bonding layer and the mixture in the pull test [40].



Figure 8. Drawing fracture surface of composite structure specimen: (a) Disconnection inside the mixture (b) Disconnection at the interface between the adhesive layer and the mixture.

Table 3. The number of interface disconnections between the bonding layer and the mixture of the composite structure specimens under different working conditions.

Temperature	Comparison Group				High Temperature Loading, Salt Spray Erosion Group			
	1.5%	3.0%	4.5%	6.0%	1.5%	3.0%	4.5%	6.0%
25 °C	0	0	2	5	0	0	4	8
60 °C	1	1	3	7	1	1	6	8

It can be seen from Table 3 that under the same conditions of temperature and curing mode, as the porosity of the mixture increases, the number of interface disconnections between the bonding layer of the composite structure specimen and the mixture increases. Under the condition of 25 °C, at the porosity of 3% and below, the number of disconnections between the bonding layer and the mixture interface of each group of composite structure specimens is 0, and under the condition of 60 °C, at the porosity of 3% and below, the number of breaks between the bonding layer and the mixture interface of each group of composite structure specimens is 1 time; under the conditions of 4.5% and at the porosity of 6.0%, the number of disconnection between the bonding layer and the mixture interface of each group of composite structure specimens increased significantly. It is proved that when the porosity of the mixture is 3% and below, the mixture can better protect the interface and ensure good interface bonding performance between the composite structure bonding layer and the mixture.

Under the same temperature conditions, when the porosity is 4.5% and 6.0%. Comparing the comparison group with the high temperature loading and salt spray erosion groups, the high temperature loading and salt spray erosion groups have a higher number of interface disconnections, indicating that high temperature loading and salt spray erosion have a greater influence on the interface disconnection between the bonding layer of the composite structure and the mixture. When the grade segregation of the mixture causes a large porosity or a large porosity, the interface bonding performance of the composite

structure bonding layer and the mixture will be greatly attenuated under the external high temperature and high salt conditions.

Under the same conditions of porosity and curing method, when the test temperature rises from 25 °C to 60 °C, the number of interface disconnections between the composite structure bonding layer and the mixture increases, indicating that the temperature has a greater influence on the interface disconnection between the bonding layer of the composite structure and the mixture; at the same time, the number of disconnection of composite structure specimens with low porosity ($\leq 3.0\%$) is less, and the number of disconnection of composite structure specimens with high porosity ($\geq 4.5\%$) is more.

Therefore, the porosity of the epoxy asphalt mixture should be controlled within 3.0% seeing from the perspective of ensuring the interlayer bonding performance.

3.2. Rust on the Surface of the Steel Plate

After the pull test is completed, pry open the composite structure specimens under different working conditions, clean up the epoxy resin adhesive layer on the surface of the steel plate, and compare and observe the compactness of the interlayer concrete surface and the corrosion of the steel plate surface after the composite structure under different working conditions is pried open, which is shown in Figures 9 and 10.

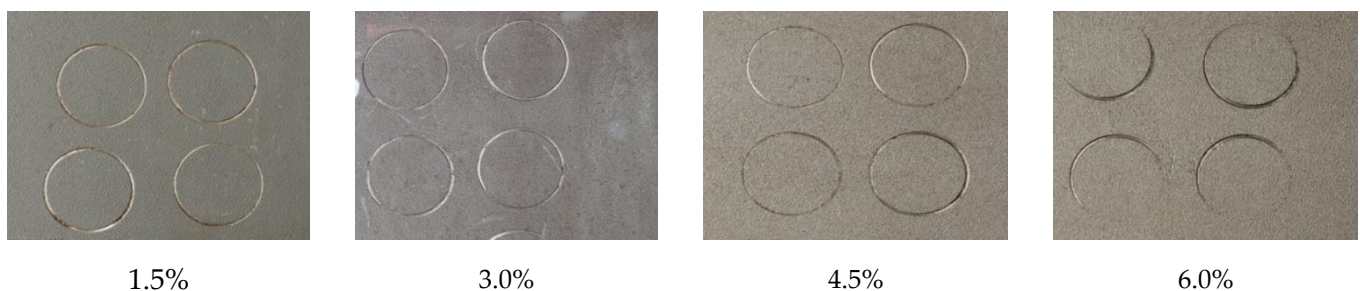


Figure 9. Rust on the surface of steel plate (comparison group).

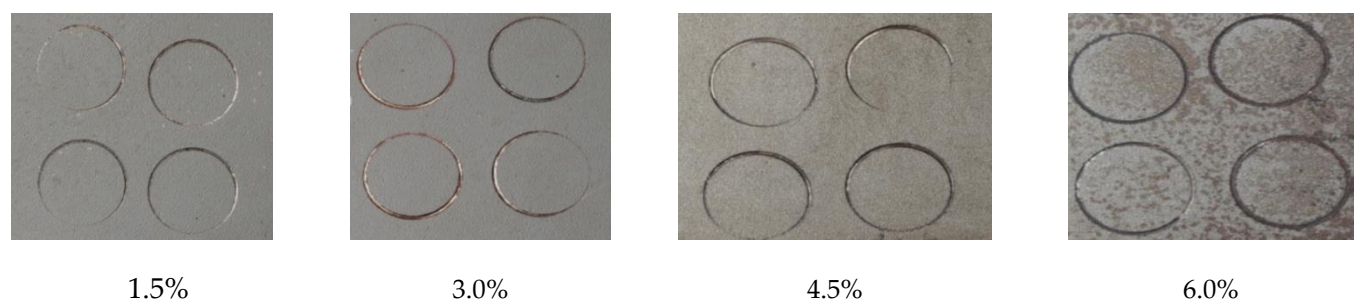


Figure 10. Rust condition on the surface of steel plate (high temperature loading and salt spray erosion group).

Through tests and observations, it is found that when the porosity of epoxy asphalt mixture is 1.5% and 3%, there is no trace of corrosion on the surface of the steel plate. When the porosity is 4.5% and 6%, the surface of the steel plate has more corrosion, and the corrosion is more serious under the condition of 6% of porosity than under the condition of 4.5% of porosity; high temperature loading and salt spray erosion and curing will aggravate this situation. Considering the protection of steel plates, the porosity of epoxy asphalt concrete on steel bridge decks should be controlled within 3%.

Therefore, epoxy asphalt mixture should have good water tightness, and the porosity of epoxy asphalt concrete for steel bridge deck paving should be controlled within 3% to protect the steel plate from corrosion and ensure good bonding performance between layers.

4. Research on Anti-Skid Performance of Epoxy Asphalt Mixture

The service function of the bridge deck pavement determines that it should have good anti-skid performance and provide users with a safe driving environment [41–43].

According to the traditional grading curve for epoxy asphalt mixture, FAC-10 grade was used to design the pavement ratio and compares the data with the traditional EA-10C grade epoxy asphalt mixture in terms of anti-skid performance, to evaluate whether the FAC-10 grade is superior in anti-skid performance.

4.1. Anti-Skid Texture Test

The synthetic grade of FAC-10 and EA-10C is shown in Table 4. Through the design of the mix ratio, it is determined that the best oil-stone ratio of FAC-10 is 6.2%, and the best oil-stone ratio of EA-10C is 6.5%.

Table 4. Pavement layer FAC-10 synthetic grade.

Screen Hole Size (mm)	13.2	9.5	4.75	2.36	1.18	0.6	0.3	0.15	0.075
FAC-10 synthetic grade pass percentage (%)	100	98.3	43.4	31.3	22.3	17.7	14.3	11.4	8.4
EA-10C synthetic grade pass percentage (%)	100	99.3	74	57.3	39.2	29.6	22.2	16.3	11.0

A laser texture meter (see Figure 11) was used to test the depth of the two-graded three-dimensional structure, the angle between the peaks of the pavement structure profile, and the density of the micro-texture distribution. The test results of FAC-10 and EA-10C are shown in Tables 5 and 6, respectively. The laser texture images of FAC-10 and EA-10C are shown in Figures 12 and 13, respectively.

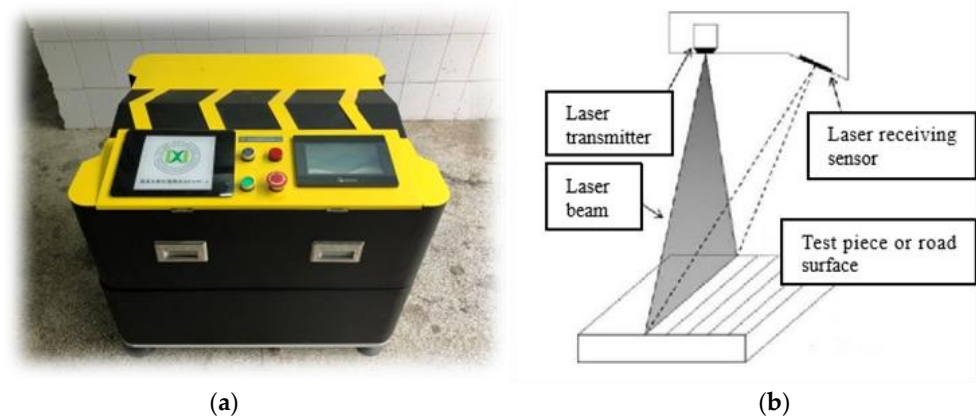


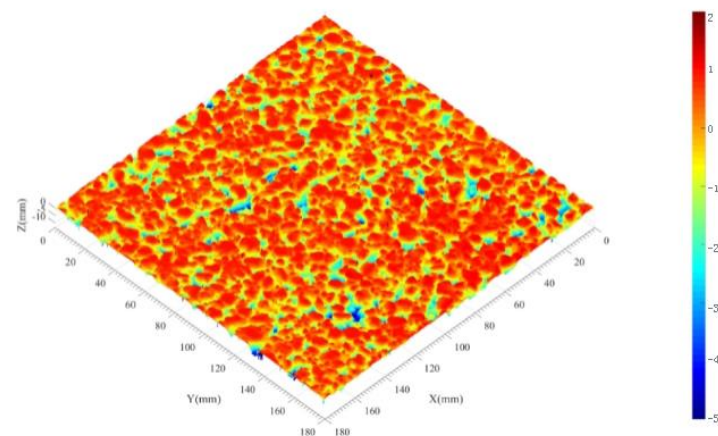
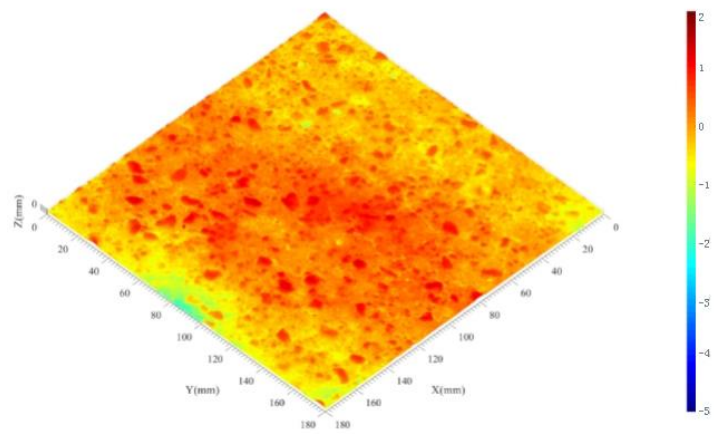
Figure 11. Pavement anti-skid texture tester: (a) Laser texture meter (b) Schematic diagram of scanning principle.

Table 5. Results for FAC-10 laser texture detection.

S/N	Three-Dimensional Structure Depth (mm)	Included Angle of Profile Peak (Proportion of Each Interval)				Micro Texture Distribution Density
		0~45°	45~90°	90~135°	135~180°	
1	0.76	0.42%	4.62%	35.49%	59.46%	1.68
2	0.76	0.52%	6.16%	35.02%	58.31%	1.84
3	0.74	0.21%	2.82%	27.18%	69.79%	1.52
4	0.86	0.32%	4.34%	33.15%	62.19%	1.66
5	0.92	0.47%	4.54%	35.07%	59.92%	1.73
6	1.05	0.33%	4.12%	34.01%	61.54%	1.63
Average value	0.85	0.38%	4.43%	33.32%	61.87%	1.68

Table 6. Results for EA-10C laser texture detection.

S/N	Three-Dimensional Structure Depth (mm)	Included Angle of Profile Peak (Proportion of Each Interval)				Micro Texture Distribution Density
		0~45°	45~90°	90~135°	135~180°	
1	0.27	0.00%	0.02%	2.04%	97.94%	1.09
2	0.24	0.00%	0.02%	7.31%	92.67%	1.14
3	0.32	0.00%	0.01%	1.67%	98.31%	1.09
4	0.25	0.00%	0.02%	1.79%	98.18%	1.05
5	0.37	0.00%	0.00%	2.97%	97.03%	1.1
6	0.34	0.00%	0.01%	2.96%	97.03%	1.1
Average value	0.30	0.00%	0.01%	3.12%	96.86%	1.1

**Figure 12.** Laser texture image of FAC-10 detection point.**Figure 13.** Laser texture image of EA-10C detection point.

4.2. Anti-Skid Performance Analysis

The average structural depth of FAC-10 is 0.85 mm, the average structural depth of EA-10C is 0.3 mm, and the structural depth of FAC-10 is about 2.8 times that of EA-10C.

According to the tire/road anti-skid mechanism, the more the edges and corners of the pavement structure are, and the deeper the structure peak penetrates the tread rubber, the greater the cutting plough force will be [44–46]. In addition, when the pavement structure is sharper, it can better pierce the water film under the wet condition of the pavement, which is beneficial to improve the anti-skid performance of the asphalt pavement under wet conditions [47,48]. It can be seen from Tables 5 and 6 that the percentage of the acute angle value of the peak-top angle of the FAC-10 pavement structure profile is 4.81%, while the percentage of the acute angle value of the peak-top angle of the EA-10C pavement structure

profile is only 0.01%. The top angle of the surface structure of the EA-10C section is mainly between 135° – 180° accounting for 96.86%, that is, the angle of the top of the structure profile is mainly an obtuse angle, which is consistent with the distribution of EA-10C in the actual road surface with more scum.

From the analysis of the micro-texture density test results in Tables 5 and 6, it can be seen that the EA-10C section is close to a smooth plane (the micro-structure distribution density is 1.1, which is close to 1.0), while the micro-texture distribution density of FAC-10 is 1.68, which is significantly larger than the micro-texture distribution density of EA-10C.

Compared with EA-10C, FAC-10 has obvious advantages in anti-skid performance.

5. Summary and Conclusions

This paper was conducted to comprehensively study the integrated design of structural and material of epoxy asphalt mixture used in steel bridge deck pavement. The work done by this study yields the following conclusions:

- Under relatively unfavorable conditions, the tensile strain on the top surface of the steel bridge deck pavement is lower than $300\ \mu\epsilon$, and the maximum PP peak amplitude is $427\ \mu\epsilon$, which is significantly lower than the $600\ \mu\epsilon$ fatigue endurance limit of hot-mix epoxy asphalt concrete;
- The epoxy asphalt mixture should have good water tightness, and the porosity of epoxy asphalt concrete for steel bridge deck paving should be controlled within 3% to protect the steel plate from corrosion and ensure good bonding performance between layers;
- The structural depth of epoxy asphalt mixture FAC-10 is about 2.8 times that of EA-10C. Additionally, the micro-texture distribution density of FAC-10 is significantly greater than that of EA-10C. The percentage of acute angle value of the peak-top angle of the pavement structure profile of FAC-10 is 4.81%, while that of EA-10C is only 0.01%.

The ultimate strain level of fatigue endurance for epoxy asphalt mixture is higher than that of the steel bridge deck. Considering the flexural and tensile fatigue performance, the use of a hot-mix epoxy asphalt mixture for steel deck pavement is recommended because it can ensure longer life in theory. Besides, the epoxy asphalt mixture has good flexibility and significant water tightness, which can adapt to the following deformation of the steel plate and ensure that the steel plate interface is not corroded and has good bonding performance. Moreover, the porosity of epoxy asphalt mixture used in steel bridge deck paving is recommended to be controlled within 3%. Finally, in terms of the anti-skid performance of bridge deck pavement, the FAC-10 graded epoxy asphalt mixture is recommended when compared with EA-10C.

Future investigations will focus on the comparison between typical mixtures used for bridge applications such as EA-10C and FAC-10 in terms of fatigue endurance and interfacial bonding performance.

Author Contributions: Conceptualization, W.N. and D.W.; methodology, W.N. and Y.S.; software, W.X.; validation, W.X. and X.X.; formal analysis, W.N.; investigation, X.X.; data curation, W.N.; writing—original draft preparation, W.N. and W.X.; writing—review and editing, W.N. and Y.S.; supervision, W.N. and D.W.; project administration, D.W.; funding acquisition, D.W. All authors have read and agreed to the published version of the manuscript.

Funding: This research was funded by the Natural Science Fund of Guangdong Province, grant number 2019A1515011965, and Natural Science Foundation of China, grant number 51808228.

Institutional Review Board Statement: Not applicable.

Informed Consent Statement: Not applicable.

Data Availability Statement: The data presented in this study are available on request from the corresponding author.

Conflicts of Interest: The authors declare no conflict of interest.

References

1. Wang, Z.; Zhang, S. Fatigue endurance limit of epoxy asphalt concrete pavement on the deck of long-span steel bridge. *Int. J. Pavement Res. Technol.* **2018**, *11*, 408–415. [\[CrossRef\]](#)
2. He, Q.; Zhang, H.; Li, J.; Duan, H. Performance evaluation of polyurethane/epoxy resin modified asphalt as adhesive layer material for steel-UHPC composite bridge deck pavements. *Constr. Build. Mater.* **2021**, *291*, 123364. [\[CrossRef\]](#)
3. Wang, S.; Zhang, C.; Pan, Z.; Sun, D.; Zhou, A.; Xie, S.; Wang, J.; Zou, J. Microplastics in wild freshwater fish of different feeding habits from Beijiang and Pearl River Delta regions, south China. *Chemosphere* **2020**, *258*, 127345. [\[CrossRef\]](#) [\[PubMed\]](#)
4. Woo, M.-K.; Huang, L.; Zhang, S.; Li, Y. Rainfall in Guangdong province, South China. *CATENA* **1997**, *29*, 115–129. [\[CrossRef\]](#)
5. Dębska, B.; Licholai, L.; Miąsik, P. Assessment of the Applicability of Sustainable Epoxy Composites Containing Waste Rubber Aggregates in Buildings. *Buildings* **2019**, *9*, 31. [\[CrossRef\]](#)
6. Getahun, M.A.; Shitote, S.M.; Gariy, Z.C.A. Experimental Investigation on Engineering Properties of Concrete Incorporating Reclaimed Asphalt Pavement and Rice Husk Ash. *Buildings* **2018**, *8*, 115. [\[CrossRef\]](#)
7. Chen, J.; Dan, H.; Ding, Y.; Gao, Y.; Guo, M.; Guo, S.; Han, B.; Hong, B.; Hou, Y.; Hu, C.; et al. New innovations in pavement materials and engineering: A review on pavement engineering research 2021. *J. Traffic Transp. Eng.* **2021**, *8*, 815–999. [\[CrossRef\]](#)
8. Bheel, N.; Tafsirojjaman, T.; Liu, Y.; Awoyera, P.; Kumar, A.; Keerio, M.A. Experimental Study on Engineering Properties of Cement Concrete Reinforced with Nylon and Jute Fibers. *Buildings* **2021**, *11*, 454. [\[CrossRef\]](#)
9. Li, Y.; Cao, D.; Zhang, Y.; Jia, X. Performance of a dry-method-epoxy modifier and a modified epoxy-asphalt mixture. *Constr. Build. Mater.* **2021**, *266*, 120229. [\[CrossRef\]](#)
10. Ghassemirad, A.; Bala, N.; Hashemian, L.; Bayat, A. Application of asphaltenes in high modulus asphalt concrete. *Constr. Build. Mater.* **2021**, *290*, 123200. [\[CrossRef\]](#)
11. Yu, H.; Zhu, Z.; Leng, Z.; Wu, C.; Zhang, Z.; Wang, D.; Oeser, M. Effect of mixing sequence on asphalt mixtures containing waste tire rubber and warm mix surfactants. *J. Clean. Prod.* **2020**, *246*, 119008. [\[CrossRef\]](#)
12. Zhang, H.; Mao, Q.; Zhu, Z.; Zhang, Z.; Pan, Y.; Wan, J.; Zhou, C.; Qian, J. Experimental study on service performance of epoxy asphalt steel deck pavement of cable stayed bridge. *Case Stud. Constr. Mater.* **2020**, *13*, e00392. [\[CrossRef\]](#)
13. Xu, P.; Cong, P.; Li, D.; Zhu, X. Toughness modification of hyperbranched polyester on epoxy asphalt. *Constr. Build. Mater.* **2016**, *122*, 473–477. [\[CrossRef\]](#)
14. Chelelgo, K.; C. Abiero Gariy, Z.; Muse Shitote, S. Laboratory Mix Design of Cold Bitumen Emulsion Mixtures Incorporating Reclaimed Asphalt and Virgin Aggregates. *Buildings* **2018**, *8*, 177. [\[CrossRef\]](#)
15. Wang, T.; Wei, X.; Zhang, D.; Shi, H.; Cheng, Z. Evaluation for Low Temperature Performance of SBS Modified Asphalt by Dynamic Shear Rheometer Method. *Buildings* **2021**, *11*, 408. [\[CrossRef\]](#)
16. Li, D.; Leng, Z.; Zou, F.; Yu, H. Effects of rubber absorption on the aging resistance of hot and warm asphalt rubber binders prepared with waste tire rubber. *J. Clean. Prod.* **2021**, *303*, 127082. [\[CrossRef\]](#)
17. Yu, H.; Leng, Z.; Zhang, Z.; Li, D.; Zhang, J. Selective absorption of swelling rubber in hot and warm asphalt binder fractions. *Constr. Build. Mater.* **2020**, *238*, 117727. [\[CrossRef\]](#)
18. Xu, C.; Wang, D.; Zhang, S.; Guo, E.; Luo, H.; Zhang, Z.; Yu, H. Effect of Lignin Modifier on Engineering Performance of Bituminous Binder and Mixture. *Polymers* **2021**, *13*, 1083. [\[CrossRef\]](#)
19. Yu, H.; Leng, Z.; Dong, Z.; Tan, Z.; Guo, F.; Yan, J. Workability and mechanical property characterization of asphalt rubber mixtures modified with various warm mix asphalt additives. *Constr. Build. Mater.* **2018**, *175*, 392–401. [\[CrossRef\]](#)
20. Yu, H.; Deng, G.; Zhang, Z.; Zhu, M.; Gong, M.; Oeser, M. Workability of rubberized asphalt from a perspective of particle effect. *Transp. Res. Part D Transp. Environ.* **2021**, *91*, 102712. [\[CrossRef\]](#)
21. Wu, C.; Wu, P.; Wang, J.; Jiang, R.; Chen, M.; Wang, X. Ontological knowledge base for concrete bridge rehabilitation project management. *Autom. Constr.* **2021**, *121*, 103428. [\[CrossRef\]](#)
22. Li, Y.; Li, L.; Bindiganavile, V. Constitutive Model of Uniaxial Compressive Behavior for Roller-Compacted Concrete Using Coal Bottom Ash Entirely as Fine Aggregate. *Buildings* **2021**, *11*, 191. [\[CrossRef\]](#)
23. Yan, H.; Cai, M.; Song, S.; Huang, Y.; Fan, X.; Ye, X.; Li, H.; Li, W.; Zhu, M. Self-dispersing complex lithium-based thickener fiber for high-performance anti-corrosion/wear epoxy coating filler. *Appl. Surf. Sci.* **2021**, *563*, 150221. [\[CrossRef\]](#)
24. Chen, J.; Wang, J.; Zhu, J.-H.; Feng, Y.; Liu, C.-B. Study on the Corroded Hollow Section RC Columns Strengthened by ICCP-SS System. *Buildings* **2021**, *11*, 197. [\[CrossRef\]](#)
25. He, Z.-Q.; Ou, C.; Tian, F.; Liu, Z. Experimental Behavior of Steel-Concrete Composite Girders with UHPC-Grout Strip Shear Connection. *Buildings* **2021**, *11*, 182. [\[CrossRef\]](#)
26. Xu, W.; Li, Z.; Zhang, X. Research on Orthogonal Anisotropic Steel Bridge Decks and Analysis of Design Elements. *J. China Foreign Highw.* **2006**, *26*, 175–179.
27. Ahmed, F.; Thompson, J.; Kim, D.; Huynh, N.; Carroll, E. Evaluation of pavement service life using AASHTO 1972 and mechanistic-empirical pavement design guides. *Int. J. Transp. Sci. Technol.* **2021**. [\[CrossRef\]](#)
28. Liu, C.; Qian, Z.; Liao, Y.; Ren, H. A Comprehensive Life-Cycle Cost Analysis Approach Developed for Steel Bridge Deck Pavement Schemes. *Coatings* **2021**, *11*, 565. [\[CrossRef\]](#)
29. Qian, Z.; Li, Z.; Chen, C. Fracture criterion for mode I crack of epoxy asphalt concrete paving course of steel deck bridge pavement. *China J. Highw. Transp.* **2008**, *21*, 33–38.

30. Xu, X.; Gu, Y.; Huang, W.; Chen, D.; Zhang, C.; Yang, X. Structural Optimization of Steel—Epoxy Asphalt Pavement Based on Orthogonal Design and GA—BP Algorithm. *Crystals* **2021**, *11*, 417. [\[CrossRef\]](#)
31. Geng, T.; Chen, S.; Zhao, L.; Zhang, Z. Research on Bonding Performance of Anchorage Caisson Foundation with Different Contact Surfaces and Grouting Bed. *Buildings* **2021**, *11*, 365. [\[CrossRef\]](#)
32. Yu, S.; Ou, J. Fatigue life prediction for orthotropic steel deck details with a nonlinear accumulative damage model under pavement temperature and traffic loading. *Eng. Fail. Anal.* **2021**, *126*, 105366. [\[CrossRef\]](#)
33. Zhu, X.; Zhang, Q.; Chen, L.; Du, Z. Mechanical response of hydronic asphalt pavement under temperature–vehicle coupled load: A finite element simulation and accelerated pavement testing study. *Constr. Build. Mater.* **2021**, *272*, 121884. [\[CrossRef\]](#)
34. Fan, X.; Luo, R. Experimental study on crack resistance of typical steel-bridge-deck paving materials. *Constr. Build. Mater.* **2021**, *277*, 122315. [\[CrossRef\]](#)
35. Misaghi, S.; Tirado, C.; Nazarian, S.; Carrasco, C. Impact of pavement roughness and suspension systems on vehicle dynamic loads on flexible pavements. *Transp. Eng.* **2021**, *3*, 100045. [\[CrossRef\]](#)
36. Liu, Y.; Qian, Z.; Shi, X.; Zhang, Y.; Ren, H. Developing cold-mixed epoxy resin-based ultra-thin antiskid surface layer for steel bridge deck pavement. *Constr. Build. Mater.* **2021**, *291*, 123366. [\[CrossRef\]](#)
37. Tahmasebinia, F.; Wang, Y.; Wu, S.; Ho, J.; Shen, W.; Ma, H.; Sepasgozar, S.M.E.; Marroquin, F.A. Advanced Structural Analysis of Innovative Steel–Glass Structures with Respect to the Architectural Design. *Buildings* **2021**, *11*, 208. [\[CrossRef\]](#)
38. Yu, H.; Leng, Z.; Zhou, Z.; Shih, K.; Xiao, F.; Gao, Z. Optimization of preparation procedure of liquid warm mix additive modified asphalt rubber. *J. Clean. Prod.* **2017**, *141*, 336–345. [\[CrossRef\]](#)
39. Zhang, S.; Wang, D.; Guo, F.; Deng, Y.; Feng, F.; Wu, Q.; Chen, Z.; Li, Y. Properties investigation of the SBS modified asphalt with a compound warm mix asphalt (WMA) fashion using the chemical additive and foaming procedure. *J. Clean. Prod.* **2021**, *319*, 128789. [\[CrossRef\]](#)
40. Park, J.K.; Kim, M.O. The effect of different exposure conditions on the pull-off strength of various epoxy resins. *J. Build. Eng.* **2021**, *38*, 102223. [\[CrossRef\]](#)
41. Wu, X.; Zheng, N.; Lei, J. Influencing factors and mechanism for the attenuation of the skid resistance for bauxite clinker-asphalt mixtures. *Constr. Build. Mater.* **2021**, *283*, 122670. [\[CrossRef\]](#)
42. Peng, C.; Hu, X.; You, Z.; Xu, F.; Jiang, G.; Ouyang, H.; Guo, C.; Ma, H.; Lu, L.; Dai, J. Investigation of anti-icing, anti-skid, and water impermeability performances of an acrylic superhydrophobic coating on asphalt pavement. *Constr. Build. Mater.* **2020**, *264*, 120702. [\[CrossRef\]](#)
43. Yu, H.; Zhu, Z.; Zhang, Z.; Yu, J.; Oeser, M.; Wang, D. Recycling waste packaging tape into bituminous mixtures towards enhanced mechanical properties and environmental benefits. *J. Clean. Prod.* **2019**, *229*, 22–31. [\[CrossRef\]](#)
44. Guo, F.; Pei, J.; Zhang, J.; Li, R.; Zhou, B.; Chen, Z. Study on the skid resistance of asphalt pavement: A state-of-the-art review and future prospective. *Constr. Build. Mater.* **2021**, *303*, 124411. [\[CrossRef\]](#)
45. Chu, L.; Cui, X.; Zhang, K.; Fwa, T.F.; Han, S. Directional Skid Resistance Characteristics of Road Pavement: Implications for Friction Measurements by British Pendulum Tester and Dynamic Friction Tester. *Transp. Res. Rec.* **2019**, *2673*, 793–803. [\[CrossRef\]](#)
46. Liang, J.; Gu, X.; Deng, H.; Ni, F. Detecting device and technology of pavement texture depth based on high precision 3D laser scanning technology. *IOP Conf. Ser. Mater. Sci. Eng.* **2019**, *652*, 012063. [\[CrossRef\]](#)
47. Qian, Z.-d.; Liu, Y.; Liu, C.-b.; Zheng, D. Design and skid resistance evaluation of skeleton-dense epoxy asphalt mixture for steel bridge deck pavement. *Constr. Build. Mater.* **2016**, *114*, 851–863. [\[CrossRef\]](#)
48. Uz, V.E.; Gökalp, İ. Comparative laboratory evaluation of macro texture depth of surface coatings with standard volumetric test methods. *Constr. Build. Mater.* **2017**, *139*, 267–276. [\[CrossRef\]](#)